Int. J. Electrochem. Sci., 11 **(2016)** 2686 - 2708

International Journal of
ELECTROCHEMICAL
SCIENCE
www.electrochemsci.org

Preparation and Evaluation of Nickel Oxide-Carbon Nanotube Supported Palladium as Anode Electrocatalyst for Formic Acid Fuel Cells

S. S. Hossain[1,*], *J. Saleem*[2], *A. Al. Ahmed*[3], *M.M. Hossain*[4], *M. N. Shaikh*[5], *S. U. Rahman*[6], *G. Mc Kay*[7]

[1]College of Engineering, King Faisal University, Hofuf-31982, Kingdom of Saudi Arabia
[2]Department of Chemical Engineering, University of Karachi, Pakistan
[3]CoRE Renewable Energy, [4]Department of Chemical Engineering, and [5]CENT, King Fahd University of Petroleum & Minerals, Dhahran 31261, Saudi Arabia
[6]Midad Chemicals Company Limited, Al-Khobar, Saudi Arabia
[7]Division of Sustainable Development, College of Science, Engineering and Technology, Hamad Bin Khalifa University, Qatar Foundation, Doha, Qatar
[*]E-mail: snooruddin@kfu.edu.sa

Received: 19 October 2015 / *Accepted:* 22 December 2015 / *Published:* 1 March 2016

In this study, promotional effects of NiO on Pd/NiO-CNT catalysts (CNT: carbon nanotubes) for formic acid oxidation is investigated. Firstly, NiO is loaded on CNT in various amounts by precipitation-deposition method using urea as precipitating agent, and then palladium is deposited on the NiO-CNT support material by the borohydride reduction method. The synthesized catalysts are characterized by XRD, SEM-EDX, TEM, N_2 adsorption-desorption and XPS for their morphology, composition and electronic structure. Cyclic voltammetry, chronoamperometry, and carbon monoxide stripping voltammetry reveal that the addition of NiO enhances the electrocatalytic activity and stability of Pd/NiO-CNT catalysts remarkably. Highest current density (80.83 mA/cm^2) is achieved for the catalyst with 15 wt. % NiO content which is three times higher than the current density shown by Pd/CNT (23.23 mA/cm^2). The maximum power density in passive direct formic acid fuel cell is found to be 13.6 and 6.2 mW/cm^2 for Pd/15% NiO-CNT and Pd/CNT, respectively, which clearly demonstrate the beneficial effect of addition of NiO on Pd/NiO-CNT. The improvement in the electrocatalytic activity and stability is ascribed to the formation of small and highly dispersed Pd particles and the modification of electronic structure of Pd in presence of NiO.

Keywords: Nickel oxide; Carbon nanotubes; Palladium-electrocatalyst; Passive formic acid fuel cell

1. INTRODUCTION

In recent years direct formic acid fuel cells (DFAFCs), which use formic acid as anode feed, are gaining major attention. DFAFCs are attractive because formic acid is relatively less toxic, and have limited fuel cross over though the membrane during the fuel cell operation, which is a serious concern in other liquid fuel cells like methanol and ethanol fuel cells[1-4]. Low crossover through membrane allows DFAFCs to be operated at high formic acid concentration to compensate its low energy density compared to methanol. Therefore, it can provide high power densities at low temperature [2]. Furthermore, recent studies have shown that formic acid can be produced at large scale by the electrochemical reduction of carbon dioxide (CO_2)[5, 6]. With the possibility of using solar energy for the electrochemical reduction of CO_2, DFAFCs can serve dual purpose of storing intermittent solar energy as well as to utilize greenhouse CO_2 gas.

Despite its attractive advantages, one serious drawback with DFACs is the slow kinetics of formic acid oxidation (FAO) reaction at the anode. Electrocatalysts containing platinum (Pt) and palladium (Pd) have been found to be effective in accelerating FAO reaction [2, 7, 8]. Generally, Pd promotes direct oxidation of formic acid to CO_2, whereas Pt tends to favor the indirect pathway, which involves carbon monoxide (CO) as intermediate specie [7-9]. However, both Pd and Pt show low stability due to the poisoning of the active metals by CO generated during the during the FAO reaction [4, 7, 10, 11]. Moreover, it is widely accepted that the addition of some metals or organic ligands can enhance the performance of the electrocatalysts. Remarkable improvement in the electrocatalytic activity and stability has been reported when Pt-based catalysts are modified with metals and organic ligands, sometimes exceeding the performance of Pd based electrocatalysts[12-16]. But, relative to Pt, Pd is cheaper and more abundant, and displays higher inherent catalytic activity towards FAO. Therefore, Pd-based electrocatalysts are preferred over Pt-based electrocatalysts. It has been reported that addition of another metal (Ni, Fe, Co, Pb, Ir, Sn, & Au) to Pd further improves the catalytic activity and stability for FAO[17-23]. Nevertheless, satisfactory level of catalytic activity, long-term stability and cost reduction necessary for commercialization of the DFAFCs has not been achieved yet.

In addition to the active metals, support materials also have considerable effect on the performance of the electrocatalysts for fuel cells[24, 25]. Carbon[26-28] , carbon nanotubes (CNTs)[11, 22, 23, 29-31], mesoporous carbon[32], carbon nanofibers[33, 34], and graphene[4, 35, 36] are common support material for DFAFCs electrocatalysts. Carbon nanotubes have generally shown better performance compared to conventional carbon support for electrocatalysts for methanol, ethanol, and formic acid fuel cells.

Addition of metal oxides to the carbonaceous supports has been shown to impart beneficial effect on their performance as electrocatalyst. Transition metal oxides are particularly attractive because of their low cost, high stability and high oxygen carrying capacity. Cerium oxide[10], titanium oxide[37], aluminum oxide[38], manganese oxide[39], molybdenum oxide[40], tungsten oxide[31, 41-43], and europium oxide[44] have been shown to greatly improve the catalytic activity of the electrocatalysts for FAO. To the best of knowledge of the authors, application of nickel oxide (NiO) modified CNTs as support material for electrocatalysts for DFAFCs has not been reported in the literature.

The objective of the present research is to study the promotional effects of NiO on the electrocatalytic activity of Pd-NiO/CNT catalysts for FAO reaction and to optimize the NiO content to achieve high activity. The amount of NiO was varied from 5- 30 wt. %, while the Pd loading was kept at 20 wt. % in all the catalysts. The microstructure and composition of the synthesized catalysts were characterized by scanning electron microscopy (SEM), X-ray diffraction (XRD), energy dispersive X-ray spectroscopy (EDX), transmission electron microscopy (TEM), X-ray photoelectron spectroscopy (XPS), and nitrogen adsorption/desorption isotherm. The electrocatalytic activity of the catalysts were evaluated by cyclic voltammetry (CV), chronoamperometry (CA) and CO stripping voltammetry tests. Finally, the Pd/15%NiO-CNT and Pd/CNT were compared in an air breathing passive DFAFC using polarization and power density curves.

2. EXPERIMENTAL

2.1 Chemicals

Multiwall carbon nanotubes (MWCNTs) (with purity greater than 99.9% and BET surface area of 300 m^2/g) were purchased from Cheap Tubes Inc®. Multiwall carbon nanotubes (MWCNTs) will be referred to as CNT throughout the text for brevity. Nickel nitrate hexahydrate ($Ni(NO_3)_2.\ 6H_2O$, 99.9%), palladium nitrate dihydrate ($Pd(NO_3)_2.2H_2O$, 40 wt. %Pd), tri-sodium citrate dihydrate ($HOC(COONa)(CH_2COONa)_2.2H_2O$ and sodium borohydride ($NaBH_4$) were purchased from Merck®. Sulfuric acid (H_2SO_4, 97–98 wt.%), formic acid (HCOOH, 95 wt.%), ethanol (C_2H_5OH, 99.8 wt.%), hydrochloric acid (HCl, 37 wt.%) and Nafion resin (5 wt.% solution in aliphatic alcohols and water) were purchased from Sigma Aldrich®. Millipore water was used for the preparation of all aqueous solutions. All reagents were used as received without further purification.

2.2 Catalyst preparation

2.2.1 Preparation of NiO-CNT composite

The CNTs were acid group functionalized using nitric acid and sulfuric acid by following the procedure outlined previously[45]. Nickel oxide was deposited on CNTs by homogeneous deposition precipitation method (HDP) using urea as precipitating agent[46]. In a typical synthesis procedure, required amount of nickel nitrate was added in a constantly stirred suspension made by adding 0.8 g functionalized CNTs in 200 ml deionized water. The suspension was acidified ($pH \sim 2-3$) by adding few drops of nitric acid. The suspension was heated to 90 °C, and subsequently, 30 ml of 0.42 M aqueous urea solution was added dropwisely. The suspension was maintained at 90 °C for 6 hours with vigorous stirring for deposition to take place. At the end of 6 hours, the suspension becomes neutral ($pH \sim 7$), which indicates that urea was completely hydrolyzed. The slurry was cooled to room temperature, centrifuged, thoroughly washed with deionized water and dried at 70°C for 8 hours in a vacuum oven. The powder was calcined in a tubular furnace at 400 °C for 3 hours under high purity

argon flow of 100 ml/min. By following the same procedure with different amount of nickel nitrate, support materials with 5, 10, 15, 20, & 30 wt % NiO were synthesized.

2.2.1 Preparation of Pd/NiO-CNT electrocatalysts

As synthesized NiO-CNT was used as support material for the electrocatalyst and Pd, the active metal, was deposited on the support by wet impregnation method using sodium borohydride as reducing agent. The procedure outlined by Zhang et al. [47] was followed with slight modification. In a typical synthesis procedure, 150 mg of the support material was suspended in 100 ml of 3:1(v/v) water and ethanol mixture and sonicated for 30 minutes. Separately, appropriate amount of tri-sodium citrate dihydrate was dissolved in 10 ml water-ethanol solution. The sodium citrate solution was added to the support suspension and stirred for 1 hour. The required amount of the precursor salt was dissolved in 50 ml of water-ethanol solution separately. The solution was added dropwisely to the support suspension under constant stirring. The suspension was sonicated for 1 hour, and further stirred for another three hours to achieve a homogenous suspension. A few drops of 5 % NaOH was used to adjust the pH of the mixture to near neutral ($pH \sim 7$). Freshly prepared solution of sodium borohydride, prepared by dissolving 120 mg of sodium borohydride in 10 ml water-ethanol mixture, was added to the support suspension dropwisely under vigorous stirring. The suspension was vigorously stirred for 10 hours to make sure that all precursor salts were reduced to metal particles. Finally, the suspension was cooled to room temperature, centrifuged, thoroughly washed with deionized water and dried at 70 °C for 8 hours under vacuum to get the final catalyst. A total of 20 wt% loading of Pd in all the electrocatalyst was desired.

2.3. Catalyst characterizations

X-ray diffraction patterns of catalyst were collected in order to characterize phase, crystallinity and size of the catalyst particles. XRD analysis of the prepared catalyst was performed by a Rigaku diffractometer (D/MAX-IIIA, 3 kW) using CuK_α radiation (40 kV, 30 mA, λ = 0.1543 nm) to record the diffraction patterns between $20° \geq 2\theta \geq 80°$.

The Bruauner, Emett, Teller (BET) surface area, pore volume, and average pore radius of the CNTs and the prepared electrocatalysts were measured by recording the N_2 adsorption-desorption isotherm at 77 K using ASAP-2020 system from Micrometrics®. Prior to the analysis, the samples were degassed at 200 °C for 5 hours under 50 mTorr vacuum.

The morphology of the prepared electrocatalysts was investigated by using a field emission scanning electron microscope (FESEM) (JEOL JSM-6460LV) operated at 20 KV equipped with energy dispersive X-ray (EDX). Transmission electron microscopy (TEM) images were obtained with high resolution field emission transmission electron microscope at 200 kV using JEOL JEM-2100F. Sample for TEM and SEM was prepared by sonicating one milligram of the catalyst in 10 mL of ethanol for 30 min and then an aliquot of the suspension was placed on a an aluminum foil which was mounted on the sample holder by means of a double sided adhesive copper tape.

X-ray photoelectron spectroscopy (XPS) was carried out using a VG scientific ESCALAB MKII spectrometer equipped with a dual aluminum-magnesium anode X-ray gun and a 150-mm concentric hemispherical analyzer using Al-Ka ($h\upsilon$ =1486.6 eV) radiation from an anode operated at 130W.

2.4. Electrochemical measurements

Cyclic voltammetry (CV), chronoamperometry (CA) and CO stripping experiments were carried out to ascertain the overall electrocatalytic activity of the prepared electrocatalysts. All the above mentioned electrochemical experiments were performed with PGSTAT 302 (Metrohm-Autolab, Netherlands) at room temperature in a 250 ml standard three-electrode cell. Glassy carbon (3 mm diameter) electrode coated with a thin layer of electrocatalyst was used as working electrode. A Pt mesh connected with Pt wire (8 cm length, 1.23 mm dia.) and Ag/AgCl (3.5 M KCl) electrode was used as the counter and reference electrodes, respectively. Active surface area of the working electrode and counter electrode were 0.071 cm^2 and 8.0 cm^2, respectively. All the potentials in this study are reported with respect to Ag/AgCl electrode (3.5 M KCl) unless otherwise mentioned. The GC electrode was polished to a mirror finish with of 0.3 μ and 0.05 μ alumina powder and sonicated for 15 min in ethanol first and then in millipore water before every experiment. At first 5 mg of the electrocatalyst was dispersed in 1 mL of ethanol, and 30 μL 5 wt. % Nafion solution by sonication for 30 min to form catalyst ink. Ten micro liters of the catalyst ink was transferred (by micropipette) to the polished surface of the GC electrode and dried at 80 °C for 10 min to obtain catalyst later. For all the experiments, the Pd loading on the working electrode was maintained at 0.127 mg/cm^2. High purity nitrogen was purged through the 0.5 M H_2SO_4 solution with and without 0.5 M HCOOH for 15 min to remove dissolved air. Cyclic voltammetry experiments were performed from -0.2 to 1.2 V (vs. Ag/AgCl) at a scan rate of 20 mV/s in 0.5 M H_2SO_4 solution with and without 0.5 M HCOOH. The third cycles were recorded and used for comparison. Chronoamperometry was carried out at +0.3 V for one hour in a N_2-saturated 0.5 M H_2SO_4 + 0.5 M CHOOH solution.

Electrochemically active surface area (ECAS) and the tolerance towards CO poisoning of the catalyst samples were assessed by CO stripping voltammetry. In the stripping voltammetry, high purity N_2 was purged through the 0.5 M H_2SO_4 and 0.5 M HCOOH solution for 15 min to remove dissolved air. Subsequently, high purity CO (99.99%) was bubbled through the solution for 30 min, while the working electrode was maintained under constant applied electrode potential of -0.166 V. The solution was then purged with N_2 at the same constant potential (-0.166 V) for 30 mins to remove the dissolved CO from the solution. The CO stripping voltammograms were performed between -0.2 to 1.2 V with 20 mVs^{-1} scan rate to ensure the complete oxidation of CO_{ads}. The ECAS of Pd was estimated using two assumptions: (1) there was a monolayer of linearly adsorbed CO and (2) the Coulombic charge required for oxidation was 0.42 mC/cm^2[43-45].

2.5. Passive fuel cells

2.5.1. Membrane electrode assembly

A membrane-electrode assembly (MEA) having an active area of 4 cm^2 was fabricated using Nafion® 117 membrane**.** The membrane was pretreated before being used in the MEA. The membrane was washed with millipore water and boiled in 5 wt.% H_2O_2 for one hour. Then it was flushed with water several times and again boiled in 0.5 M H_2SO_4 solution for one hour to exchange Na^+ with H^+. The membrane was rinsed with water again to complete the pretreatment process. Pd/15 wt% NiO-CNT and Pd/CNT were used as anode electrocatalysts, and 60 wt.% Pt-Ru/C was used as cathode electrocatalyst. Catalyst loadings on the cathode and anode side were kept 2 mg/cm^2. Appropriate amount of the catalyst and Nafion® solution were mixed and sonicated for one hour. The prepared catalyst slurries were then coated on both the sides of the membrane. Carbon cloth (ETEK Inc.) was used as gas diffusion layer (GDL) for both anode and cathode sides. After drying, the MEAs were hot pressed in carver press at 130 °C and 2000 psi for 5 min.

2.5.2. Single cell and test conditions

Detail of the passive fuel cell used in this study can be found elsewhere [48]. In short, the MEA was sandwiched between two 1 mm thick SS 316 plates, which function as the electrical current collector. The surface of the current collector plates were coated with platinum to reduce the contact resistance with the electrodes. Several circular holes of 3 mm diameter were drilled in both current collectors to serve as the passage of formic acid and air. Two, 1 cm thick, transparent of transparent acrylic plates were used to hold the cell. The cathode side plate was open, whereas the anode side fixture housed a 3.0 ml formic acid solution reservoir. Formic acid solution diffused into the anode side of the catalyst layer of the MEA from the formic acid solution reservoir, while oxygen, from the ambient air, was diffused into the cathode catalyst layer through the holes on the current collector plates. Passive fuel cell testing was performed using An Arbin BT 2000 testing system. The polarization curves (I-V) were obtained by constant current charge/discharge measurements. A wait time of 40 s was allowed to obtain the stable voltage for each discharging current. All the experiments of the passive DFAFCs were performed at the room temperature 21-23 °C and the relative humidity of 65-71%.

3. RESULTS AND DISCUSSION

3.1. Catalyst characterizations

3.1.1. N_2 adsorption isotherms

The surface area of the electrocatalysts plays a pivotal role in their performance. Generally, support with high surface area favors the formation of well dispersed Pd nanoparticles which is

preferable for higher formic acid oxidation performance. Nitrogen adsorption-desorption isotherms were determined to investigate the textural properties of the support and the prepared electrocatalysts. Figure 1 shows the N_2 adsorption-desorption isotherms for pure CNTs and prepared electrocatalysts. All the isotherms show a typical type 1V adsorption model according to the IUPAC classifications. Table 1 summarizes the physicochemical properties, BET surface area, and pore volume for the pure CNTs and electrocatalysts.

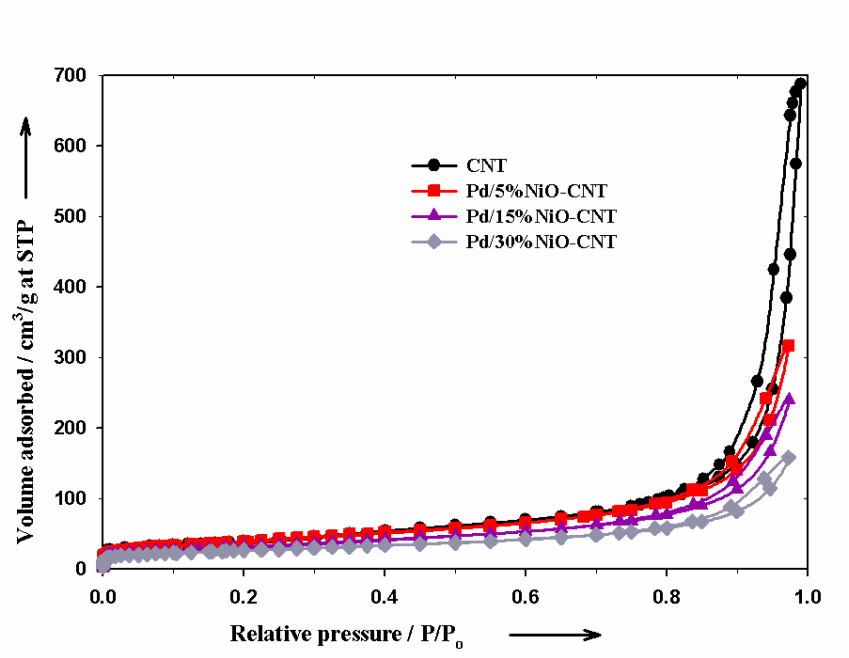

Figure 1. Nitrogen adsorption-desorption isotherm of the catalysts at 77K

With increase in the NiO content from 0% to 30% in the Pd/x NiO-CNTs electrocatalysts, BET surface area and the pore volume decreased from 300.25 to 92.55 m^2/g (Table 1). The decrease in the surface area and pore volume could be attributed to increased agglomeration and pore blocking as a result of the addition of Pd and NiO into CNTs. Although, the surface area decreased markedly upon addition of Pd and NiO, this area is still high enough to facilitate formic acid oxidation.

Table 1. Physicochemical properties of the tested catalysts

Catalysts	BET Surface Area (m^2/g)	Pore Volume (cc/g)	Mean Pore Size (nm)	Pd particle size (nm)[a]	Pd Crystallite size (nm)[b]
Pristine CNT	300.25	0.56	22.9	-	
10%NiO/CNT	257.25	0.344	5.1	-	
Pd/CNT	180	0.4	9.4	6.72	6.5
Pd/5% NiO-CNT	140.62	0.46	9.9	5.80	5.6
Pd/15% NiO-CNT	111.50	0.348	9.6	3.70	3.5
Pd/30% NiO-CNT	92.55	0.22	8.2	3.8	3.5

a =calculated from TEM, b= calculated from XRD data

3.1.2. X-ray diffraction pattern

X-ray diffraction patterns of the catalysts were collected to characterize different phases, crystallinity and crystallite size of the metal particles. Figure 2 shows the XRD patterns of 20 wt. % NiO-CNT, Pd/CNT and Pd/x NiO-CNT, catalysts prepared with different amount of NiO. The diffraction peak at 25° is found in all the samples.

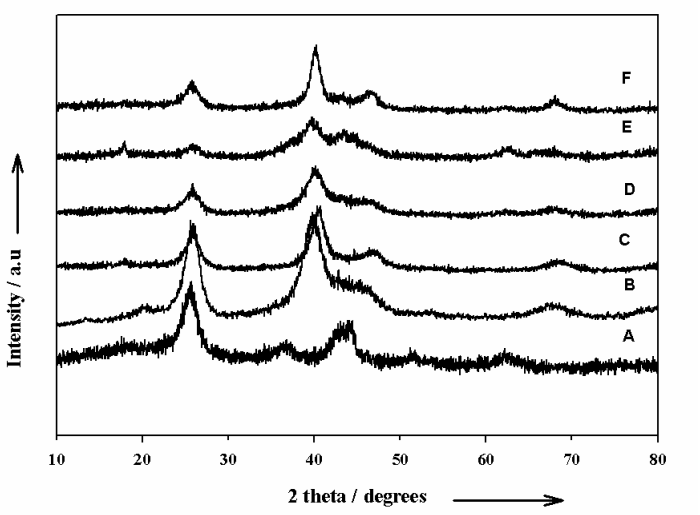

Figure 2. X-ray diffraction analysis of Pd based catalysts and support. (A) 20% NiO-CNT (B) Pd-CNT (C)Pd/5 %NiO-CNT (D)Pd-15%NiO-CNT (E) Pd/20%NiO-CNT (F) Pd/30% NiO-CNT

This peak is attributed to the hexagonal graphitic (002) plane of the graphitic carbon [43, 44]. The peak size was found of decrease with the increase of NiO loading. The surface coverage of CNT by the additional NiO and Pd is believed to be responsible for the reduction of the (022) graphitic carbon peak size. The prominent diffraction peaks at 37°, 43° and 63° (Figure. 2A) are assigned to the NiO (111),(200), and (220) planes, respectively [49, 50]. For all the catalysts, as seen in Figure.2B through Figure. 2E, the peaks at 39.8°, 47.7°and 68° correspond to the (111), (200) and (220) planes of Pd, respectively, indicating the characteristics of face-centered cubic (fcc) crystalline structure of palladium nanoparticles (JCPDS, Card No. 65-6174)[31, 50]. The presence of strong peaks of Pd (111), (200), and (220) facets in all the catalysts except, 20% NiO-CNT confirms the existence of Pd in all the samples. No detectable peak of NiO is observed in case of Pd/5% NiO-CNT (Figure. 2-C). However, the peaks become visible at higher NiO loadings (Figure 2 D-E). Absence of clear NiO peak at lower loadings might be due to the weakening of NiO peak due to the strong diffraction of Pd compared with that on the corresponding NiO-CNTs supports. Moreover, first NiO was deposited on CNTs and then Pd was loaded on the composite. Therefore, at low NiO loading (5%), Pd could cover the entire NiO which reduces the chance of NiO being detected by XRD. Similar observations also reported by Feng et al[44]. Furthermore, the Bragg's angle of Pd diffraction in Pd/NiO-CNTs was smaller than Pd/CNTs, which indicates that crystal lattice of Pd/NiO-CNTs was slightly expansive. This could be due to the strong interaction between NiO and Pd, and partial entering of NiO in Pd lattice. Similar phenomena was observed by Wang et al. [50].

The most prominent peak of Pd (111) was used to calculate the crystallite size of Pd according to the Scherrer's equation,

$$d = \frac{0.9\lambda}{\beta \cos\theta}$$

where, λ is the X-ray wavelength (1.54056 °A), θ is the Bragg angle of the peak of interest and β is the line broadening measured from the increased peak width at half height (FWHM)[50]. The results are presented in Table 1 along with the mean particle size calculated from TEM. It is also observed that Pd(111) becomes broader as the NiO content is increased (Figure 2C-E). Peak broadening of Pd (111) in Fig 2 C-E compared to Pd/CNT (Figure 2 –B), shows that NiO helps in the better dispersion of the Pd and to form smaller particle size [31]. These results are similar to the findings by Wang et al.[50] on a Pd-NiO/C catalyst. Wang et al observed that the addition of NiO to Pd/C catalysts greatly decreases the Pd particle sizes from 59.6 to 7.0 nm. Similar observations were made by Kim et al.[51], and Amin et al. [49].

3.1.3. TEM analysis

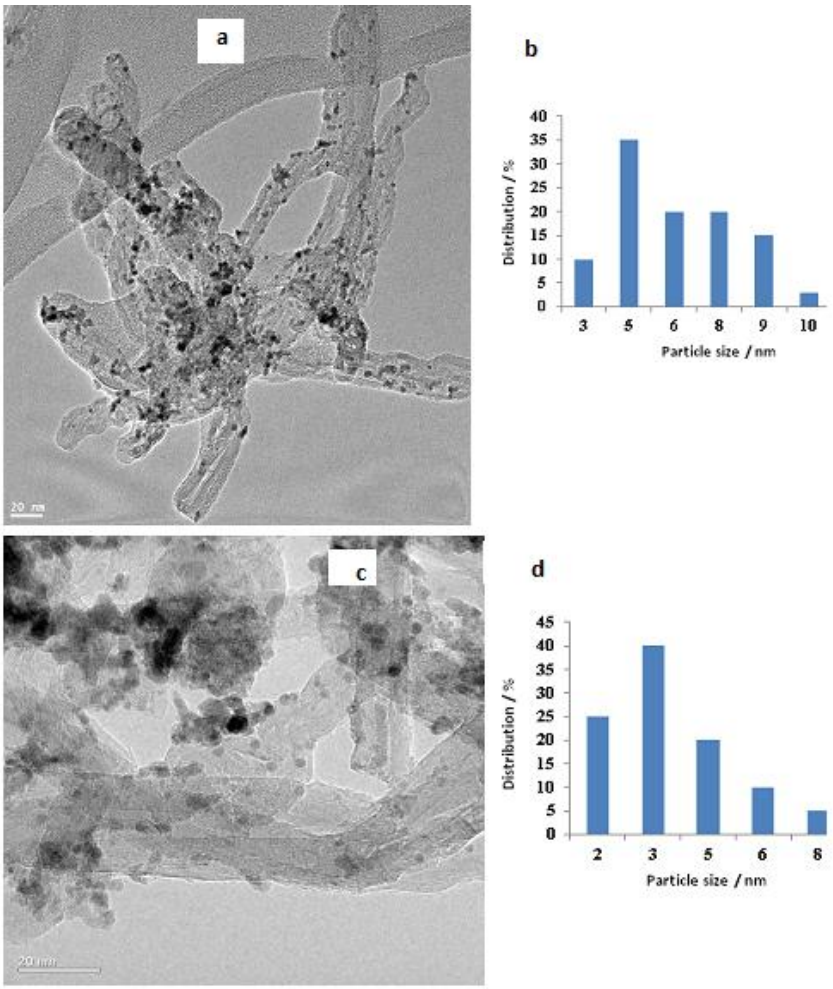

Figure 3. TEM image of Pd/CNT (A) and the histogram for particle size distribution (B); TEM image of Pd-15% NiO /CNT (C) and the histogram for particle size distribution (D)

Figure 3 displays the TEM micrographs of the Pd/CNT and Pd/15% NiO-CNT catalysts.

Figure 3A-B show the TEM image and corresponding histograms of Pd/CNT catalysts, respectively. The Pd particle sizes obtained from the TEM images are in good agreement with the Pd crystallite sizes calculated from Scherrer equation using XRD data, as summarized in Table 1. The Pd nanoparticles are found to be randomly dispersed on the wall of the characteristic tube like structure of CNTs and some of the particles agglomerated to form large particles.

Particle size ranged from 3-11 nm, with the average being 6.72 nm for Pd/CNT. In case of Pd/15% NiO-CNT, the particle size were more narrowly distributed (ranged from 2-6 nm) and the average particle size was 3.7 nm. This shows that Pd on CNTs crystals size is larger than the Pd crystals on NiO modified CNTs. Therefore, the presence of NiO minimizes the agglomeration of Pd particles on the surface of CNT support resulting in more uniformly dispersed and smaller Pd particles.

3.1.4. SEM-EDX analysis

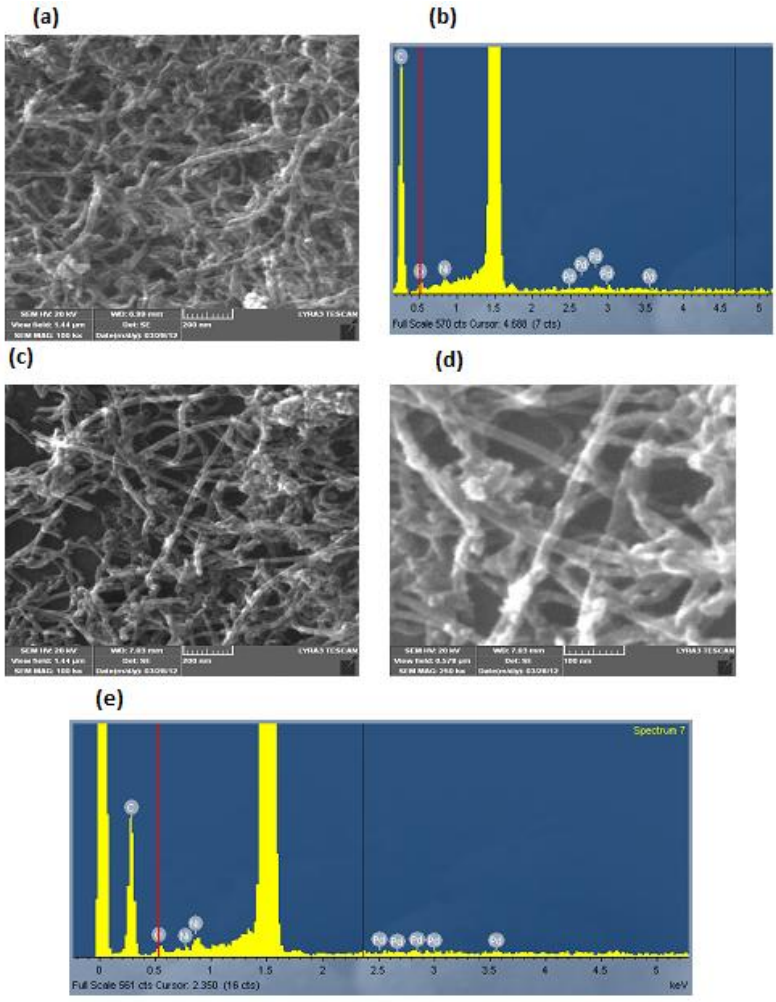

Figure 4. High magnification SEM-EDX for (A-B) Pd/5% NiO-CNT (C-E) Pd/15%NiO-CNT

The morphology and elemental analysis of the catalysts were investigated using SEM-EDX analysis. The corresponding results are shown in Figure 4.

Tube like structure of CNTs is clearly visible in all the catalysts. Nanosized metal particles can be seen to be deposited on the surface of the CNTs. The three-dimensional structure of the CNTs, small particles size and high dispersion of catalyst (Pd) nanoparticles could result in large catalyst surface area and good electrocatalytic properties for FAO. Moreover, for the catalyst samples with high NiO (>20%) contents, large agglomerations of metal oxide and metal particles are visible. On the other hand, from the EDX results shown in Figure 4b, Pd, is confirmed that Ni, C and O_2 are the present in Pd/NiO-CNT electrocatalyst. Oxygen (O_2) may come from the nickel oxide and functionalized CNT. A large peak of Al in the spectra is because of the use of aluminum as sample holder. Therefore, the SEM-EDX result confirms that Pd and NiO were successfully deposited on the surface of CNTs and the tube like structure of the CNTs are retained. These results are consistent with the findings of the XRD results.

3.1.5. XPS characterization

X-ray photoelectron spectroscopy (XPS) was employed to determine the electronic property and composition of the catalyst surface. The full-scale XPS spectra for NiO-CNT, Pd/CNT and Pd/15% NiO-CNT are shown in Figure 5-A. The figure reveals the presence of carbon, nickel and oxygen in NiO-CNT, and palladium, carbon, and oxygen in Pd/CNT. Oxygen in Pd/CNTs could be from the acid functional group (-COOH) groups present on the surface of CNTs. Nickel, oxygen, palladium and carbon were found in Pd/15% NiO-CNT.

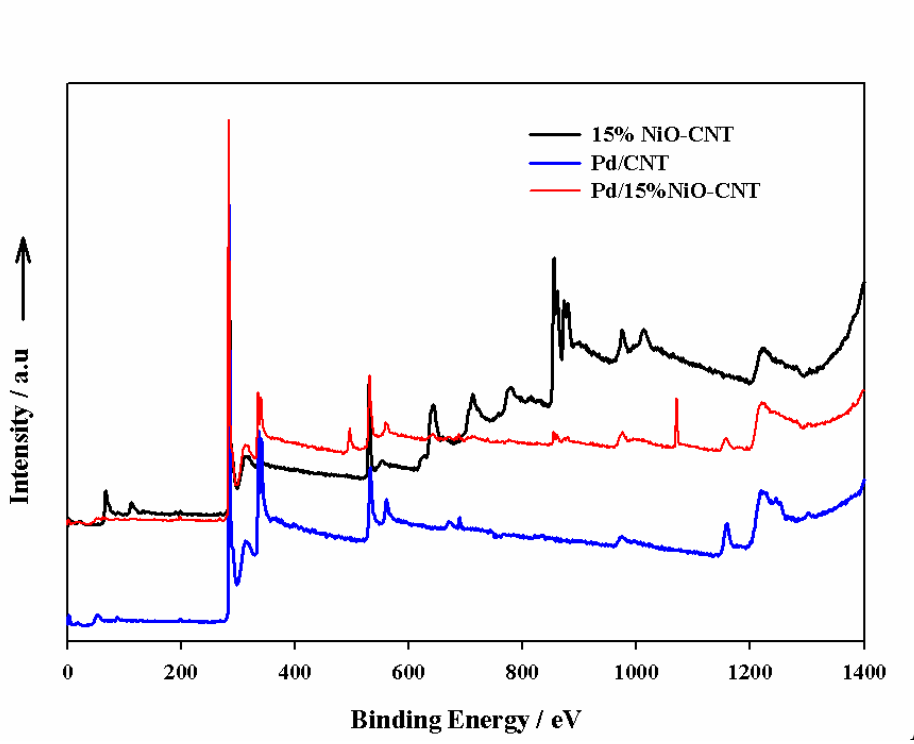

A

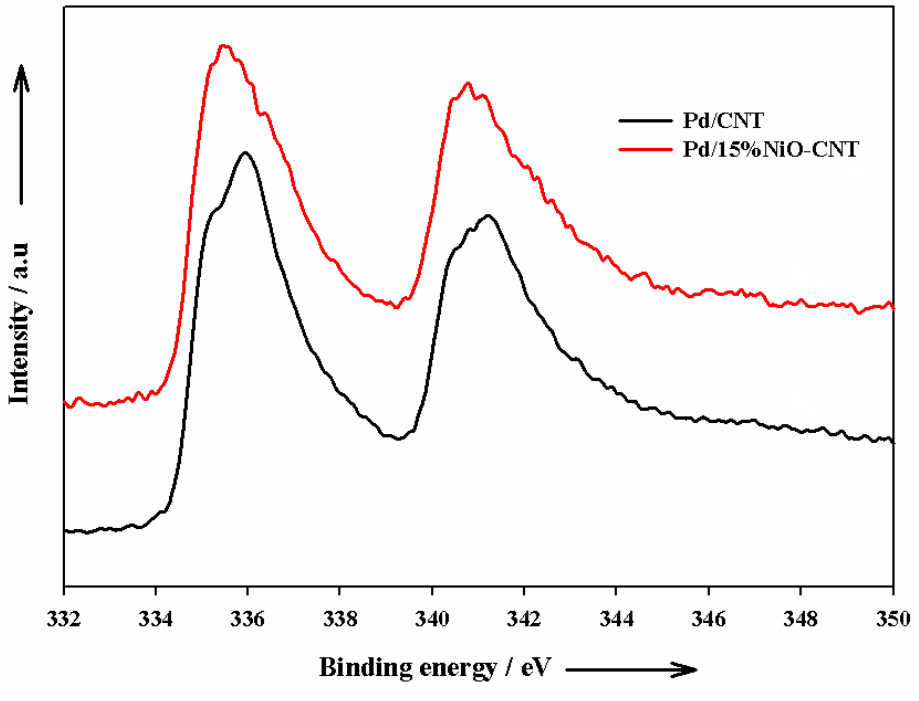

Figure 5. (A) Full range spectra of Pd/CNT and Pd/15% NiO-CNT, (B) comparision of Pd 3d peaks of Pd/CNT and Pd/15% NiO-CNT

The content of each element is 14.5% Pd, 72.3% C and 8% Ni, and 7.5 % oxygen, by weight %, respectively. In the case of Pd/CNT, 17.5% Pd, 80% C and rest oxygen. Therefore, this result further corroborates the results obtained in XRD.

Figure 5-B shows Pd(3d) regions of the XPS spectra for Pd/NiO-CNTs and Pd/CNTs. Both the spectra include a doublet that consists of a high energy peak (Pd $3d_{3/2}$) and a low energy peak (Pd $3d_{5/2}$). To analyze the peaks more accurately, the positions of Pd(3d) peaks were referred to the main peak of C(1S) (284.4 eV). The peak position for Pd $3d_{3/2}$ is found to be 335.4 and 335.9 eV for Pd/15% NiO-CNTs and Pd/CNT, respectively whereas the peak position for Pd $3d_{5/2}$ are 341.1 and 341.5 eV, respectively. It is evident that both Pd $3d_{3/2}$ and Pd $3d_{5/2}$ shifted negatively by 0.5 eV for Pd/15% NiO-CNTs compared to Pd/CNTs. The negative shift of Pd(3d) peaks is indicative of the lowering of Pd binding energy due to the addition of NiO. This behavior is typical of these types of nanoparticles and have been reported previously[21, 52, 53]. Therefore, the addition of NiO modifies the electronic structure of Pd and produces an electronic effect. The electronic effect is expected to impart beneficial effect to the electrocatalytic activity of the catalysts containing NiO and Pd. Furthermore, Zhang et al.[21] reported the lowering of Pd(3d) binding energy altered the adsorption characteristics and increased the catalytic activity of Pd/C due to the addition of tin. Similar observations were made by Li et al with the addition of Ni in the Pd supported on CNTs[22]. Therefore, it can be anticipated that in our case also the electrocatalytic activity of Pd/CNTs will be improved on addition of NiO. Moreover,

it was demonstrated by Kibler et al. that a suitable downshift of the d-band center of Pd-increased the electrocatalytic activity of the Pd for formic acid oxidation [52].

3.2. Electrochemical evaluation

3.2.1. Hydrogen adsorption-desorption

Cyclic voltammetry experiments were conducted in 0.5 M H_2SO_4 in order to evaluate the electronic and geometric structure of Pd surfaces. Cyclic voltammograms for catalysts with different NiO wt. % loadings are shown in Figure. 6. The shape of the profile is similar to the literature[7, 50, 51]. The multiple peaks between -0.2 V and +0.1V are attributed to the so called hydrogen /desorption (Hab) and hydrogen adsorption-desorption peak.

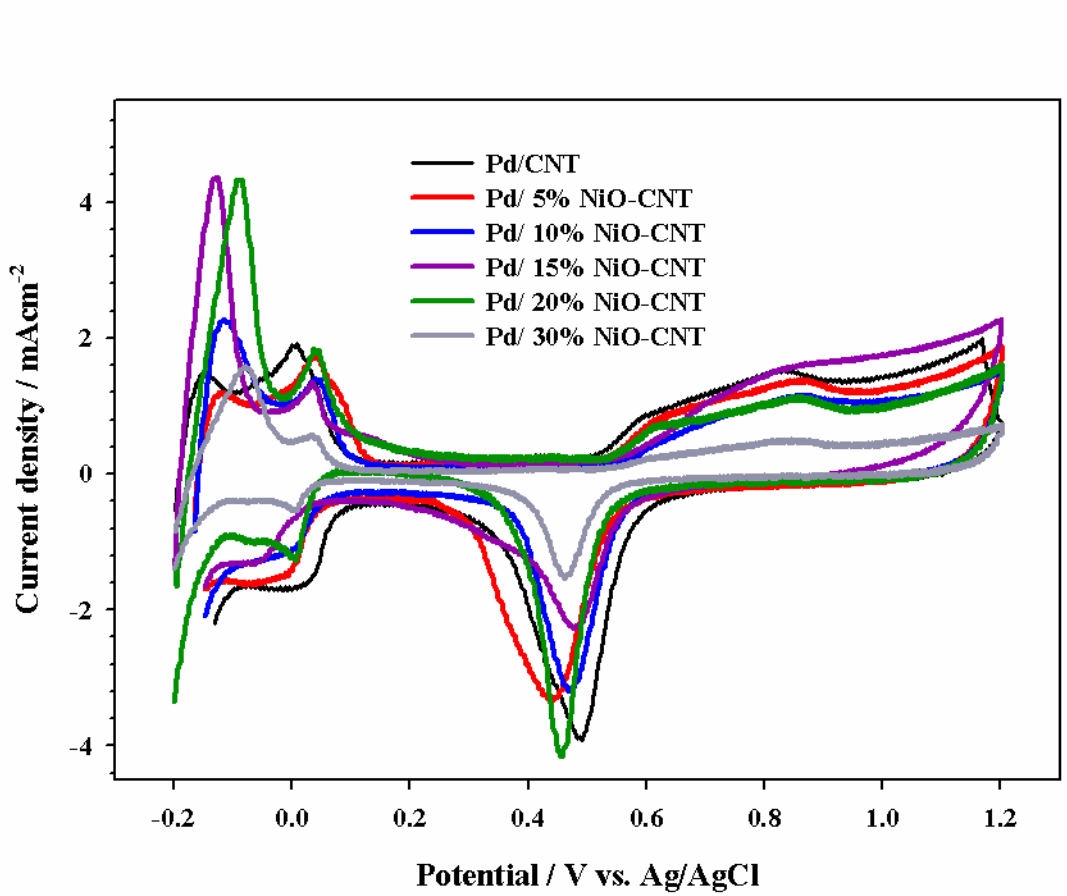

Figure 6. Cyclic voltammograms for the catalysts in 0.5 M H_2SO_4 with 20 mV/s scan rate.

The hydrogen adsorption-desorption peak in the interval of -0.2 - 0 V on Pd/NiO-CNT is larger than those on Pd/CNT. This indicates that Pd/NiO-CNT catalysts have larger ECSA, which could be due to the reduced particle size and better dispersion of the Pd nano particles. There is a prominent peak in negative scan of the CV. This peak could be attributed to the reduction of Pd oxide formed in the forward scan of the CV. In addition, the Pd surface oxide reduction peak of Pd/NiO-CNT shifts

negatively to +0.44 V from +0.5 V in Pd/CNT. This is because NiO can weaken the adsorption strength of hydrogen on the Pd surface and increases the OH adsorption strength.

3.2.2. CO stripping analysis

CO stripping cyclic voltammetry was carried out in 0.5 H_2SO_4 to evaluate CO tolerance and ECSAs of the catalysts.

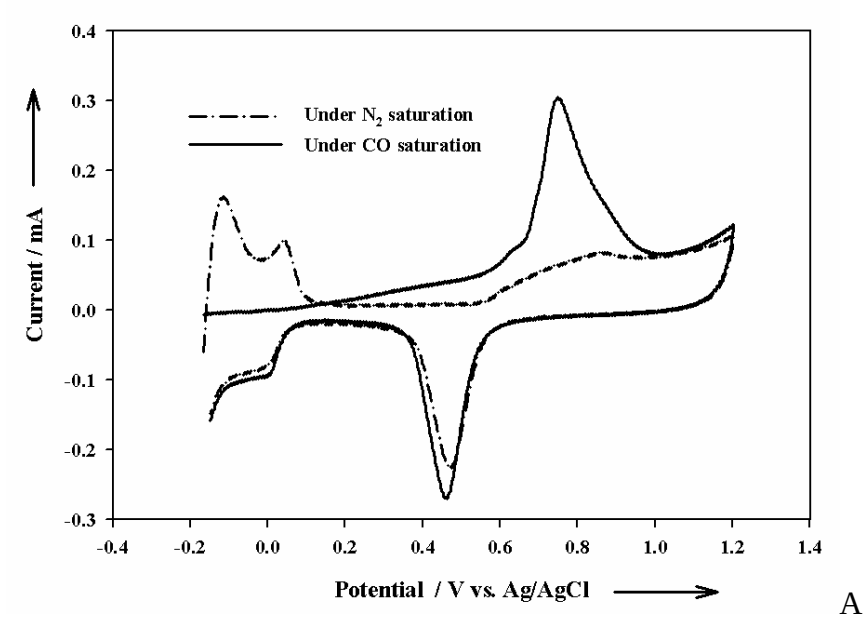

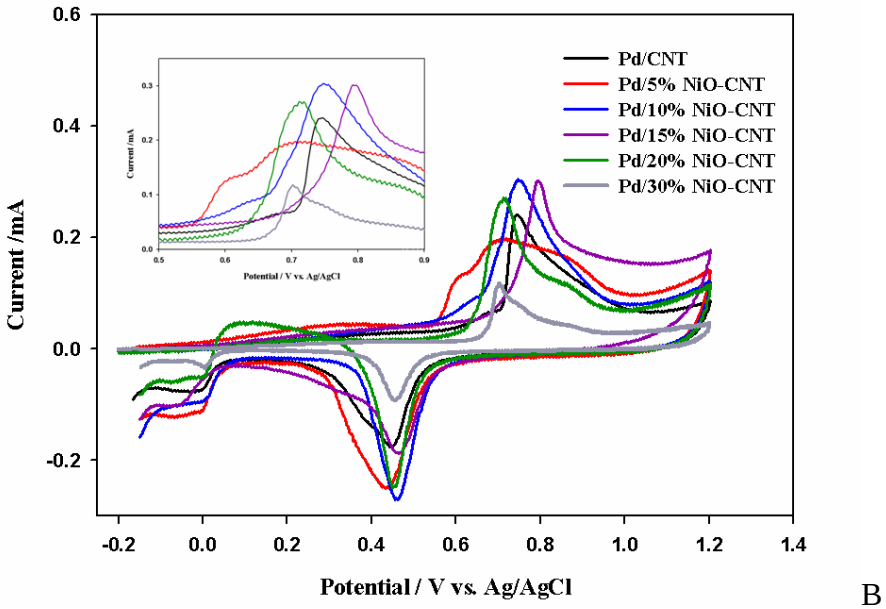

Figure 7. Cyclic voltammograms of (A) preadsorbed CO and immediate next cycle for Pd/10% NiO-CNT and (B) preadsorbed CO of Pd/CNT and all the Pd/NiO-CNT catalysts.

Figure 7 A shows the voltammograms in presence of pre adsorbed CO and the immediate next cycle for Pd/NiO-CNT. A strong and distinct oxidation peak at potential near about +0.8 V confirms the presence of adsorbed CO on the Pd surface. Moreover, no such peak was observed in the immediate next cycle, which confirms the complete removal of CO from the Pd surface during the first scan. Figure 7-B shows the CO stripping voltammograms for catalysts with different NiO loadings. A well-defined stripping peak of the adsorbed CO (CO_{ad}) is formed at the potential of approximately 0.77 V on Pd/CNTs, which illustrates that CO is strongly adsorbed on the Pd surface. In contrast, the anodic oxidation peak of CO stripping for Pd-15% NiO-CNTs is located at about 0.710 V . The peak position of CO stripping has shifted negatively by 67mV for Pd/15% NiO-CNT compared to Pd/CNT. This suggests that the addition of NiO weakens the CO adsorptive bond on the Pd active sites. The weakened strength of the CO adsorption on the Pd prevents the accumulation of the poisoning intermediates (CO) and improves the activity and stability of the catalysts[11]. Moreover, Figure 7-B shows that the area of the CO stripping peak increased steadily with the increase in the NiO content in the 20% Pd/NiO-CNT catalysts. The area of CO stripping peak was used to calculate the ECSA of the Pd nanoparticles. Table 2 summarizes the important characteristics of the CO stripping voltammograms and the ECAS of the catalysts calculated from the CO stripping measurements for all the catalysts investigated in this research. It is evident from the table that amount of NiO present in the catalysts has profound effect on the intensity of CO oxidation peaks and onset potential. Obviously, the increased ECSA at moderate NiO content is due to the smaller and well dispersed Pd nano particles in catalysts containing NiO. Thus, higher concentration of the Pd active sites are available for the electrooxidation of formic acid via direct oxidation pathway, which results in an exceptional enhancement of the electrocatalytic activity and stability.

Table 2. Electrochemical characteristics of the electrocatalysts obtained from CO stripping voltammetry**.**

Catalyst	Area of desorbed CO peak (mC/cm^2)	CO Stripping E_{onset} (mV)	E_{peak} (mV)	$ECAS_{CO}$ [a] (m^2/g metal)
Pd/CNT	27.94	580	747	52.38
Pd-5% NiO-CNT	37.11	432	712	69.57
Pd-10% NiO-CNT	34.77	480	747	65.18
Pd-15%NiO-CNT	26.44	650	710	49.56
Pd-20%NiO-CNT	30.55	454	710	57.27
Pd-30% NiO-CNT	9.88	420	700	18.52

[a] $ECAS_{CO} = \frac{\theta c}{w * 0.42}$, $\theta c = mC/cm^2$, $w = 0.127\ mg/cm^2$

3.2.3. Cyclic voltammetry analysis

Electrochemical oxidation of formic acid on Pd/x%NiO-CNT was evaluated by the cyclic voltammetry.

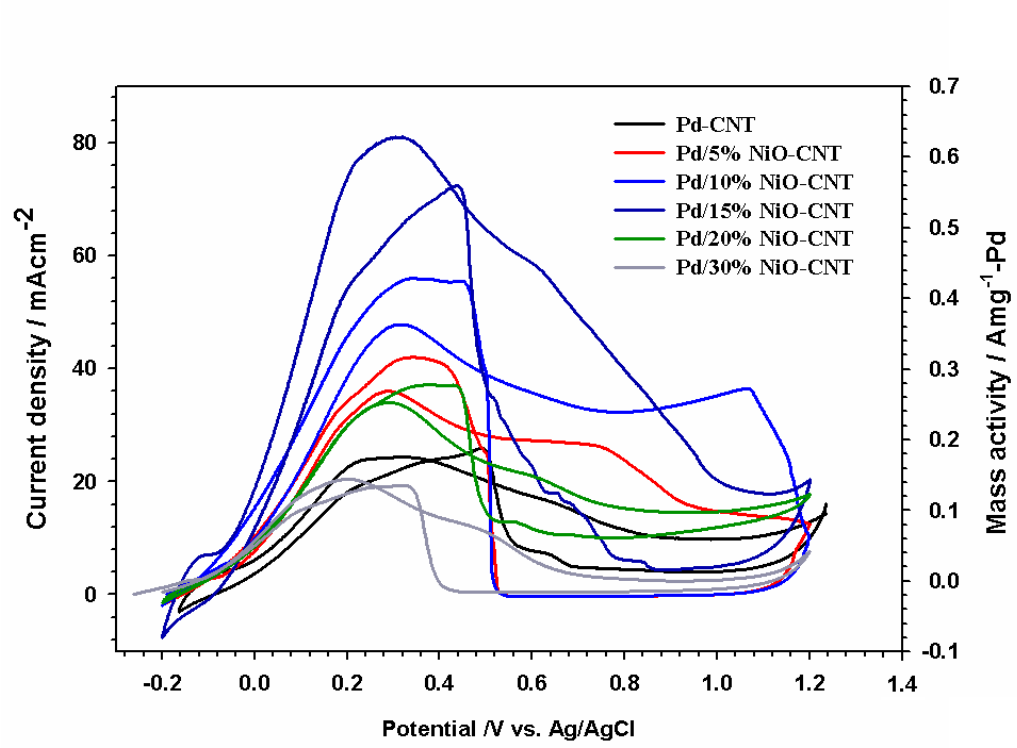

A

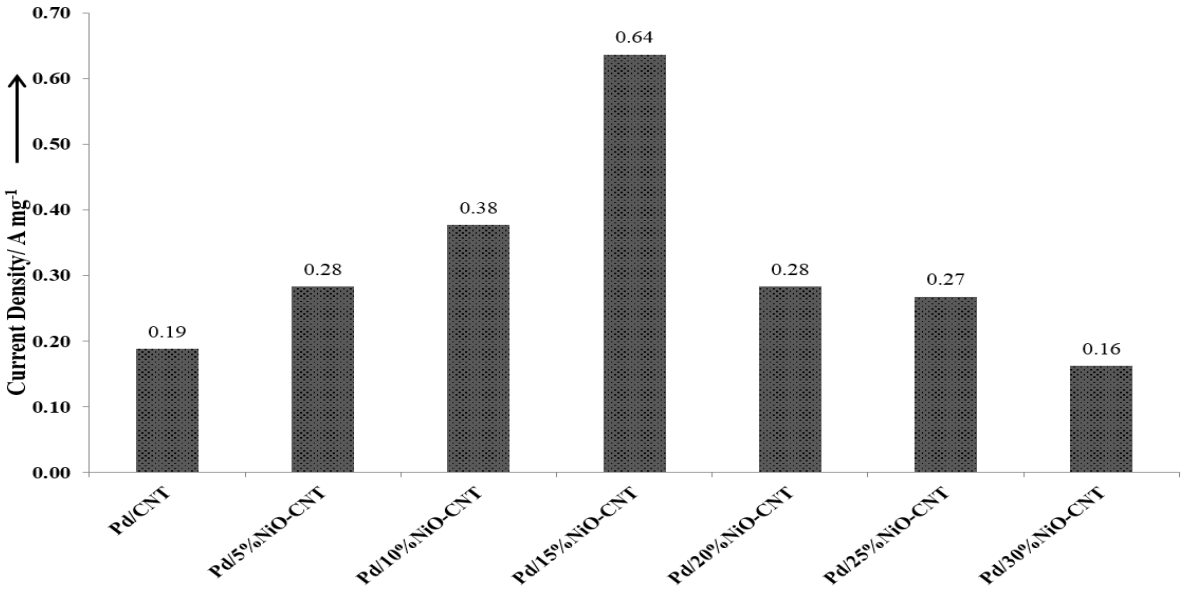

B

Figure 8. Cyclic voltammograms in 0.5 M H_2SO_4 + 0.5 M HCOOH at 20 mV/s scan rate for (A) Pd/CNT and Pd/NiO-CNT catalysts (B) Peak current density for the catalysts tested.

Figure 8 (A) shows the cyclic voltammograms (CVs) of FAO in a 0.5 M H_2SO_4+ 0.5 M HCOOH electrolyte solution on the Pd supported on NiO/CNT with different content of NiO and Pd/CNT electrodes at a scan rate of 20 mVs^{-1} in the potential range -0.2-1.2 V. Current density in Figure 8 A-B is expressed as current per unit geometric area of the GC electrode (0.071cm^2). To

further, compare the activities of catalysts, the current is normalized to the real mass of Pd metal to get the mass activity of the catalysts. It can be observed in Figure 8-A that the basic shape of voltammogram for FAO on Pd-NiO/CNT catalyst is similar to that on the Pd/CNT. In addition, in the potential range, one broad oxidation peak in the forward scan and one similar oxidation peak in the reverse scan were obtained for all the catalysts containing Pd at~ 0.3 V, which is in agreement with previous literature[10, 21, 40, 53]. The oxidation peak observed in the forward scan during the FAO reaction on Pd surface is almost exclusively by the non poison –forming direct dehydrogenation pathway, $HCOOH \rightarrow intermediate \rightarrow CO_2 + 2e^- + 2H^+$. [7, 28, 54]. The oxidation peak in the reverse scan could be attributed to the oxidation of formic acid on the regenerated Pd surface from the reduction of oxidized species of Pd, PdOH (Pd_2O) and PdO, formed in the forward scan at potentials higher than 0.7 V [19, 54]. The anodic peak current density (forward scan) reflects the amount of formic acid oxidized at the Pd electrocatalysts, and the anodic peak potential represents the ability of electrocatalysts to catalyze FAO reaction. Therefore, the anodic peak current density (or mass activity) and the peak potential are two important parameters to evaluate the electrocatalytic activity of catalysts. High value of peak current density (or mass activity) and low peak potential indicate good catalysts. It is evident from Figure 8-A that the addition of NiO in Pd/CNT catalysts increased the current density for FAO. The current densities of the main anodic peak of FAO increases sharply at Pd/10%NiO-CNT and Pd/15% NiO-CNT (47.83 and 80.83 mA/cm^2, respectively), which are 2 and 3.37 times as large as that of Pd/CNT (23.93 mA/cm^2). Similarly, peak mass activities of Pd/ 10% NiO-CNT and Pd/ 15%NiO-CNT are 0.38 and 0.64 Amg^{-1}, respectively, whereas the mass activity of Pd/CNT is 0.19 Amg^{-1}. Therefore, the activity for FAO is significantly increased by the addition of NiO in Pd/NiO-CNT compared to Pd/CNT. Many previous researches have also concluded that addition of metal oxides enhanced the electrocatalytic activity of the electrocatalyst [10, 31, 40, 41]. However, there was small positive shift of the peak position of Pd/CNT upon addition of NiO in Pd/NiO-CNT. Similar observation was made by others [34, 44, 54, 55]. Qin Li et al. attributed the positive shift in the peak potential in Pd supported on SnO_2-TiO_2 modified MWCNT to the synergic effect among the components in catalyst[34]. Zhou & Lee [55], and Feng et. al.[44] observed similar behavior and attributed the positive shift to the particle size effect. However, the positive shift in the peak potential was small and did not affect the catalytic activity much.

The optimization of the content of nickel oxide in these electrocatalysts was conducted by varying the oxide content at a fixed Pd metal loading 20% by wt. and recording the peak mass activities for FAO. The results are plotted in Figure 8B. It is clear that the content of NiO affects the peak current density for FAO with the maximum value at 15 wt. % of NiO, which is 3.37 times of Pd/CNT. Therefore, it can be concluded that moderate amount of NiO is best in enhancing the activity of the Pd/CNT catalysts.

The increased electrocatalytic activity of the Pd/NiO-CNT can be attributed to (A) increased ECSA due to the smaller particle size of the Pd crystallites (B) modification of Pd energy level due to electronic effect as revealed by the XPS analysis of the catalysts (C) presence of more oxygen –containing species provided by the NiO.

It is well known that uniformly dispersed and smaller particle size of Pd improves the catalytic activity [9, 31, 53, 55, 56]. TEM results (Table 1) show that the addition of 15 wt. % NiO to Pd/CNT

decreased the mean particle size of Pd from 6.72 to 3.7 nm, which is manifested in terms of increased ECSA. Therefore, the narrow range of particles and smaller particle size could be partially responsible for enhanced activity for FOA. However, the improved activity can not be entirely attributed to this decrease in particle size of Pd nano particles in the Pd/ NiO-CNT catalysts[10]. XPS results show that the presence of NiO modifies the electronic properties of Pd particles in Pd/NiO-CNT. This modification of the electronic structure could affect the bond energy and the interaction between HCOOH and Pd surface, which will increase the rate of FAO reaction [22, 53].

As mentioned previously that it has been accepted that electrooxidation of formic acid on the Pd supported catalysts is primarily through the direct oxidation pathway [7, 57]. Therefore, a large amount of hydrogen could occupy the Pd active sites which hinder the further adsorption of formic acid molecules. It is speculated that NiO improves the catalytic activity and CO tolerance by the same mechanism as Ru does in Pt-Ru/C during methanol oxidation. NiO, like Ru in Pt-Ru/C, generates active oxygen containing species OH_{ad} at lower potential (0.2 V). The OH_{ad} species can oxidize CO-like or other carbonaceous poisons species on the surface of Pd to CO_2, releasing the active sites Pd for further electrochemical reaction. At low oxide content, there are not enough NiO sites to effectively assist the releasing of OH_{ad} species and the oxidation current remains almost at the level obtained from pure noble metal.

The NiO content of 15% seems to present a site distribution close to the optimum for FAO. The decrease in the peak current with the further increase in the NiO content can be rationalized in terms of an inhibition of formic acid adsorption, which is probably due to the diminution of Pd active sites. In addition to this, the decline in performance with the further increase in the amount of oxide may also be due to the decrease in the electrocatalysts conductivity since NiO is a semiconductor[10, 31, 41, 44, 50, 58]. Therefore, it can be concluded that the increased activity of Pd/NiO-CNT for FAO is due to increased ECSA, electronic modification and the presence of oxygen carrying components.

3.2.4. Chronoamperometry analysis

The long-term stability (or durability) of the electrocatalytic materials is a major obstacle in the commercialization of DFAFCs. In order to evaluate the electrochemical stability of the Pd/NiO-CNT and Pd/CNT catalysts, chronoamperometry tests were conducted in 0.5 M H_2SO_4 and 0.5 M HCOOH at 0.3 V for 3600 s. This potential corresponds to the near peak current activity observed in cyclic voltammograms for most of the catalysts tested in this research. As seen from Figure 9, in both the catalysts, an initial rapid decrease in the current density was observed, followed by a slower decline in the current density.

The initial rapid decrease in current density may be due the diffusion of formic acid and the formation of poisonous intermediate species during formic acid oxidation such as CO_{ads} and CHO_{ads}.[11, 25, 59]. [59]. After several minutes, the current subsequently decreased slowly and a pseudo-steady state is achieved for the catalysts. The current density for Pd/ 15% NiO-CNT is 0.077 Amg^{-1} , which is seven times larger than the mass activity for Pd/CNT (0.011 Amg^{-1}). Therefore, it can be concluded that Pd/NiO-CNT is able to maintain current density higher than Pd/CNT. Therefore, it

can be concluded from the results of cyclic voltammetry and chronoamperometry that the addition of NiO, improves the activity as well as long- term stability of Pd/CNT.

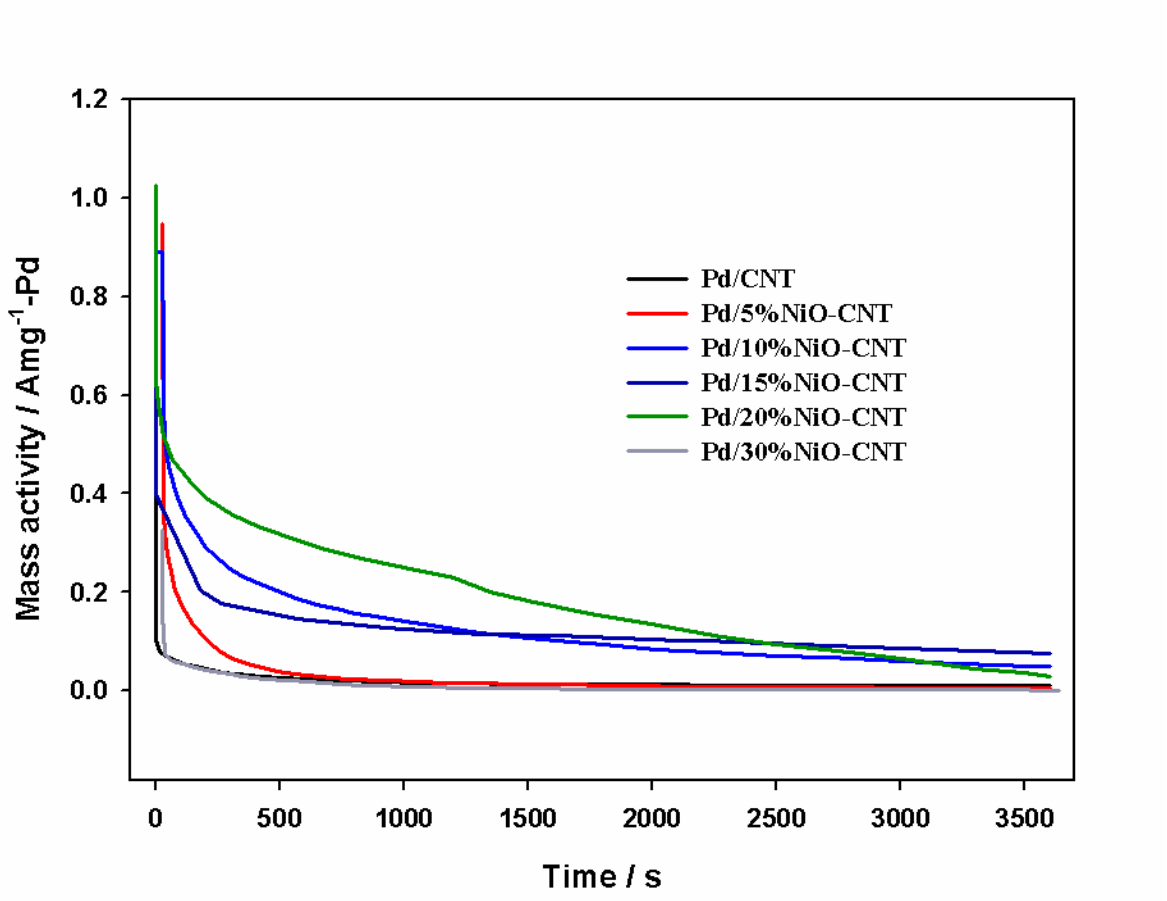

Figure 9. Chronoamperometry of 20%Pd/CNT and Pd/'15%NiO-CNT in 0.5 M H_2SO_4 and 0.5 HCOOH solution at 0.3 V

3.2.5 Passive fuel cell results

Air breathing fuel cells are suitable for portable devices as they do not require any external pumps or other auxiliary devices. Pd/CNT and Pd/15%NiO-CNT catalysts were tested in a homemade passive fuel cell system with 3 M HCOOH in the anode side and air from atmosphere in the cathode side. The polarization and power density curves of a single passive DFAFC with the two catalysts as anode are shown in Figure 10.

It was evident that the Pd/NiO-CNT catalyst showed improved performance in comparison with the Pd/CNT. The maximum power density was approximately 13.6 and 7.0 mW cm^{-2} for Pd/NiO-CNT and Pd/C catalyst, respectively. Therefore, power density increased by 1.8 factor in Pd/NiO-CNT compared to Pd/CNT. This can be attributed to the addition to NiO to Pd/CNT. Ha et al.[60] had first reported studies on the air breathing DFAFCs.

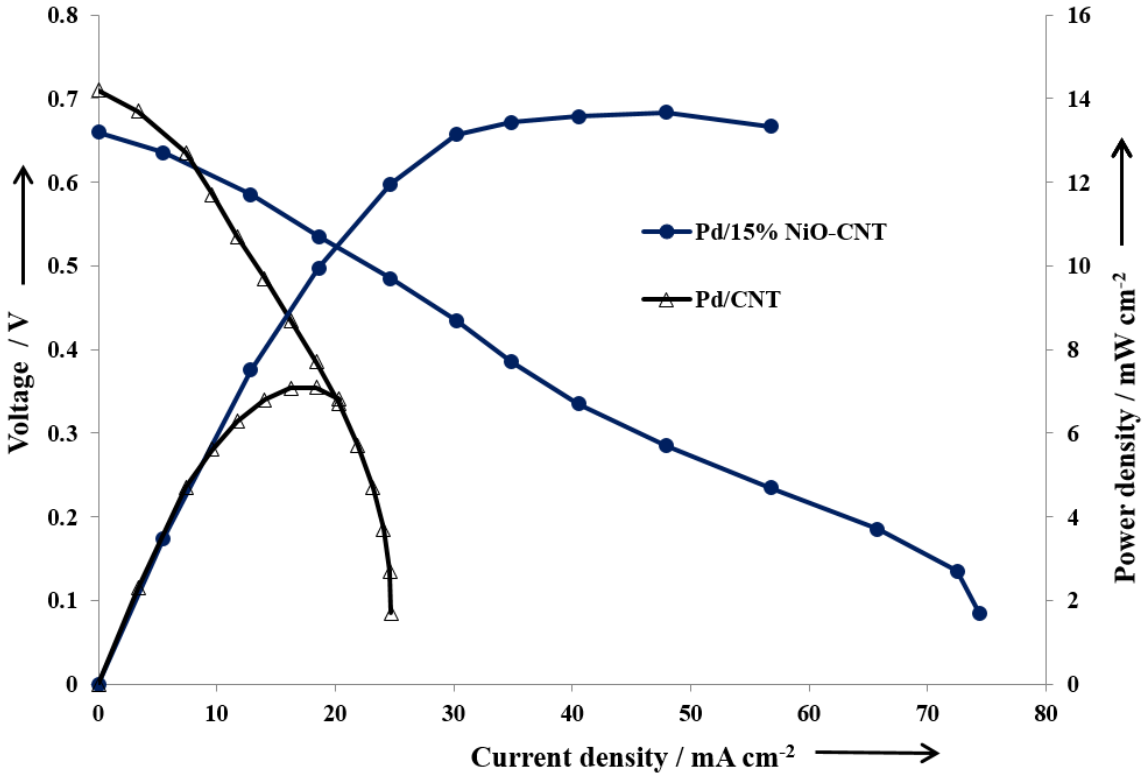

Figure 10. Polarization curves in a passive fuel cell with breathing air on the cathode side and 3 M HCOOH on the anode side.

They reported very high performance of the DFAFCs with maximum power density of 33mW/cm^2 .They used Pt black and Pt black or PtRu black (unsupported) catalysts for anode and cathode, respectively in their study. Their catalyst loading was 12 mg/cm^2. Recently, Feng et al.[41] reported the maximum power density of 7.6 mW cm^{-2} for Pd-WO_3/C under similar test condition with 4 mg/cm^2 metal loading. In our case, both the anode and cathode catalyst loading was 2 mg/cm^2. Therefore, high power density was used achieved with relatively low Pd metal loading. But, still this was a preliminary result and yet the performance was not very high for DFAFC which may be due to the low catalyst loading and not optimized MEA preparation method. However, it proves the beneficial effect of addition of NiO to Pd/CNT electrocatalysts for FAO. These results confirm the results obtained in cyclic voltammetry and chronoamperometry.

4. CONCLUSIONS

In this investigation Pd/NiO-CNT electrocatalysts with various NiO content were synthesized, characterized, and assessed using different electrochemical evaluation techniques. Following are the conclusions of this study:

1. Addition of NiO caused slight reduction in the specific surface area and pore volume of the CNTs support due to the pore blockage.

2. XRD, SEM, and TEM techniques revealed that the incorporation of NiO to the support improved the active metal, Pd, dispersion on the support surface. The nominal particle size of the active metal decreased with the increase in the NiO content in Pd/NiO-CNT catalyst sample.
3. The electrochemical tests (CV and CA) showed that Pd/NiO-CNT electrocatalysts exhibit higher electrocatalytic activity and long term stability for the electrooxidation of formic acid as compared to Pd/CNTs catalyst.
4. CO stripping results indicated that the addition of NiO in Pd/NiO-CNT increased the tolerance of the electrocatalysts towards the CO poisoning as compared to the Pd/CNT catalyst.
5. 15wt.% NiO in Pd/NiO-CNT is the optimum content of NiO for formic acid oxidation.
6. Passive fuel cell results showed power density of 13.6 mW/cm^2 for Pd/15% NiO-CNT which is two times higher than Pd/CNT.

ACKNOWLEDGEMENTS
This work was supported by the Deanship of Scientific Research at King Faisal University via annual research grant (no. 150212). The authors would also like to thank Hao Wenbin, Material Characterization and Preparation Facility (MCPF), Hong Kong University of Science & Technology, and Research Grants Council (RGC) Hong Kong.

Conflict of interest
The authors declare that we have no conflict of interest. All Authors have seen and approved the manuscript being submitted. We warrant that the article is the Authors' original work. We warrant that the article has not received prior publication and is not under consideration for publication elsewhere.

References

1. C. Rice, S. Ha, R.I. Masel, P. Waszczuk, A. Wieckowski, T. Barnard, *J. Power Sources*, 111 (2002) 83.
2. C.A. Rice, A. Bauskar, P.G. Pickup, Recent adances in electrocatalysts for formic acid oxiation, in: M. Shao (Ed.) *Electrocatalysis in Fuel Cells: A Non- and Low- Platinum Approach*, Springer-Verlag, Lonon, (2013).
3. S. Ha, R. Larsen, R.I. Masel, *J. Power Sources*, 144 (2005) 28.
4. T. Maiyalagan, X. Wang, A. Manthiram, *RSC Adv.*, 4 (2014) 4028.
5. A.B. Bocarsly, E.B. Cole, in: U.P. Office (Ed.), Princeton University, USA (2014).
6. C. Oloman, H. Li, *ChemSusChem*, 1 (2008) 385.
7. Y.X. Chen, M. Heinen, Z. Jusys, R.J. Behm, Angew. *Chem. Int. Ed. Engl.*, 45 (2006) 981.
8. S. Zhang, Y. Shao, G. Yin, Y. Lin, Angew. *Chem. Int. Ed. Engl.*, 49 (2010) 2211.
9. W.P. Zhou, A. Lewera, R. Larsen, R.I. Masel, P.S. Bagus, A. Wieckowski, *J. Phys. Chem. A*, 110 (2006) 13393.
10. L. Feng, J. Yang, Y. Hu, J. Zhu, C. Liu, W. Xing, *Int. J. Hydrogen Energy*, 37(2012) 4812.
11. O. Winjobi, Z. Zhang, C. Liang, W. Li, *Electrochim. Acta*, 55 (2011) 4217.
12. W. Zhou, J. Xu, Y. Du, P. Yang, *Int. J. Hydrogen Energy*, 36 (2011) 1903.
13. W. Zhou, Y. Du, H. Zhang, J. Xu, P. Yang, *Electrochim. Acta*, 55 (2010) 2911.
14. W. Zhou, C. Wang, J. Xu, Y. Du, P. Yang, *J. Power Sources*, 196 (2011) 1118.
15. S. Uhm, S.T. Chung, J. Lee, *Electrochem. Commun.*, 9 (2007) 2027.
16. X. Zhou, C. Liu, J. Liao, T. Lu, W. Xing, *J. Power Sources*, 179 (2008) 481.

17. Y. She, Z. Lu, W. Fan, S. Jewell, M.K.H. Leung, *J. Mater. Chem. A*, 2 (2014) 3894.
18. Y. Liu, L. Wang, G. Wang, C. Deng, B. Wu, Y. Gao, *J. Phys. Chem. C*, 114 (2010) 21417.
19. Y. Kang, L. Qi, M. Li, R.E. Diaz, D. Su, R.R. Adzic, E. Stach, J. Li, C.B. Murray, *ACS Nano*, 6 (2012) 2818.
20. X. Wang, Y. Tang, Y. Gao, T. Lu, *J. Power Sources*, 175 (2008) 784.
21. Z. Zhang, J. Ge, L. Ma, J. Liao, T. Lu, W. Xing, *Fuel Cells*, 9 (2009) 114.
22. R. Li, Z. Wei, T. Huang, A. Yu, *Electrochim. Acta*, 56 (2011) 6860.
23. D. Morales-Acosta, J. Ledesma-Garcia, L.A. Godinez, H.G. Rodriguez, L. alvarez-Contreras, L.G. Arriaga, *J. Power Sources*, 195 (2010) 461.
24. H. Huang, X. Wang, *J. Mater. Chem. A*, 2 (2014) 6266.
25. J. Chang, S. Li, L. Feng, X. Qin, G. Shao, *J. Power Sources*, 266(2014) 481.
26. P. Hong, F. Luo, S. Liao, J. Zeng, *Int. J. Hydrogen Energy*, 36 (2011) 8518.
27. Y. Gao, G. Wang, B. Wu, C. Deng, Y. Gao, *J. Appl. Electrochem*., 41 (2011) 1.
28. E. Lee, A. Murthy, A. Manthiram, *Electrochem. Commun.*, 13 (2011) 480.
29. Y.-C. Bai, W.-D. Zhang, C.-H. Chen, J.-Q. Zhang, *J. Alloy Compd*, 509 (2011) 1029.
30. M. Chen, Z.B. Wang, K. Zhou, Y.Y. Chu, *Fuel Cells*, 10 (2010) 1171.
31. C.a. Ma, Y. Jin, M. Shi, Y. Chu, Y. Xu, W. Jia, Q. Yuan, J. Chen, H. Pan, Q. Dai, *Ionics*, (2014) 1.
32. A.u. Rehman, S.S. Hossain, S.u. Rahman, S. Ahmed, M.M. Hossain, *Appl. Catal A: Gen.*, 482 (2014) 309.
33. F. Nitze, M. Mazurkiewicz, A. Malolepszy, A. Mikolajczuk, P. Kedzierzawski, C.-W. Tai, G. Hu, K.J. Kurzydlowski, L. Stobinski, A. Borodzinski, T. Wagberg, *Electrochim. Acta*, 63 (2012) 323.
34. Y.-H. Qin, J. Yue, H.-H. Yang, X.-S. Zhang, X.-G. Zhou, L. Niu, W.-K. Yuan, *J. Power Sources*, 196 (2011) 4609.
35. S. Zhang, Y. Shao, H.-g. Liao, J. Liu, I.A. Aksay, G. Yin, Y. Lin, *Chem. Mater.*, 23 (2011) 1079.
36. C. Venkateswara Rao, C.R. Cabrera, Y. Ishikawa, *J. Phys. Chem. C*, 115 (2011) 21963.
37. X.-M. Wang, J. Wang, Q.-Q. Zou, Y.-Y. Xia, *Electrochim. Acta*, 56 (2011) 1646.
38. W.-L. Qu, Z.-B. Wang, Z.-Z. Jiang, D.-M. Gu, G.-P. Yin, *RSC Adv*., 2 (2012) 344.
39. M.S. El-Deab, *J. Adv Res.*, 1 (2010) 87.
40. L. Feng, Z. Cui, L. Yan, W. Xing, C. Liu, *Electrochim. Acta*, 56 (2011) 2051.
41. L. Feng, L. Yan, Z. Cui, C. Liu, W. Xing, *J. Power Sources*, 196 (2011) 2469.
42. I.A. Rutkowska, D. Marks, C. Perruchot, M. Jouini, P.J. Kulesza, *Colloid Surface A*, 439 (2013) 200.
43. Z. Zhang, Y. Huang, J. Ge, C. Liu, T. Lu, W. Xing, *Electrochem. Commun*, 10 (2008) 1113.
44. L. Feng, S. Yao, X. Zhao, L. Yan, C. Liu, W. Xing, *J Power Sources*, 197 (2012) 38.
45. P. Serp, M. Corrias, P. Kalck, *Appl. Catal A: Gen*, 253 (2003) 337.
46. M.L. Toebes, M.K. van der Lee, L.M. Tang, M.H. Huis in 't Veld, J.H. Bitter, A.J. van Dillen, K.P. de Jong, *J. Phys. Chem. B*, 108 (2004) 1161.
47. G. Zhang, Y. Wang, X. Wang, Y. Chen, Y. Zhou, Y. Tang, L. Lu, J. Bao, T. Lu, *Appl. Catal. B-Environ*, 102 (2011) 614.
48. J.G. Liu, T.S. Zhao, R. Chen, C.W. Wong, *Electrochem Commun*., 7 (2005) 288.
49. R.S. Amin, R.M.A. Hameed, K.M. El-Khatib, M.E. Youssef, A.A. Elzatahry, *Electrochim. Acta*, 59 (2012) 499.
50. M. Wang, W. Liu, C. Huang, *Int. J. Hydrogen Energy*, 34 (2009) 2758.
51. D.B. Kim, H.-J. Chun, Y.K. Lee, H.-H. Kwon, H.-I. Lee, *Int. J. Hydrogen Energy*, 35 (2010) 313.
52. A.M. El-Aziz, L.A. Kibler, *J. Electroanal. Chem*., 534 (2002) 107.
53. R.D. Morgan, A. Salehi-khojin, R.I. Masel, *J. Phys. Chem. C* , 115 (2011) 19413.
54. H. An, H. Cui, D. Zhou, D. Tao, B. Li, J. Zhai, Q. Li, *Electrochim. Acta*, 92 (2013), 176.
55. W. Zhou, J.Y. Lee, *J. Phys. Chem. C*, 112 (2008) 3789.
56. J. Jin-nyeong, L. Hong-Gi, Y. Yeon-Tae, *Electrochem. Solid-State Lett.*, 14 (2011) B89-B91.
57. W. Chen, J. Kim, S. Sun, S. Chen, *Langmuir*, 23 (2007) 11303.

58. C. Xu, Z. Tian, P. Shen, S.P. Jiang, *Electrochim Acta*, 53 (2008) 2610.
59. C.-T. Hsieh, J.-Y. Lin, *J. Power Sources*, 188 (2009) 347.
60. S. Ha, B. Adams, R.I. Masel, *J Power Sources*, 128 (2004) 119.